THE JOURNAL OF PHYSICAL CHEMISTRY B

Article

pubs.acs.org/JPCB

# Polyelectrolyte Decomplexation via Addition of Salt: Charge Correlation Driven Zipper

Hanne S. Antila and Maria Sammalkorpi*

Department of Chemistry, Aalto University, P.O. Box 16100, 00076 Aalto, Finland

Supporting Information

**ABSTRACT:** We report the first atomic scale studies of polyelectrolyte decomplexation. The complex between DNA and polylysine is shown to destabilize and spontaneously open in a gradual, reversible zipper-like mechanism driven by an increase in solution salt concentration. Divalent $CaCl_2$ is significantly more effective than monovalent NaCl in destabilizing the complex due to charge correlations and water binding capability. The dissociation occurs accompanied by charge reversal in which charge correlations and ion binding chemistry play a key role. Our results are in agreement with experimental work on complex dissociation but in addition show the underlying microstructural correlations driving the behavior. Comparison of our full atomic level detail and dynamics results with theoretical works describing the PEs as charged, rigid rods reveals that although charge correlation involved theories provide qualitatively similar responses, considering also specific molecular chemistry and molecular level water contributions provides a more complete understanding of PE complex stability and dynamics. The findings may facilitate controlled release in gene delivery and more in general tuning of PE membrane permeability and mechanical characteristics through ionic strength.

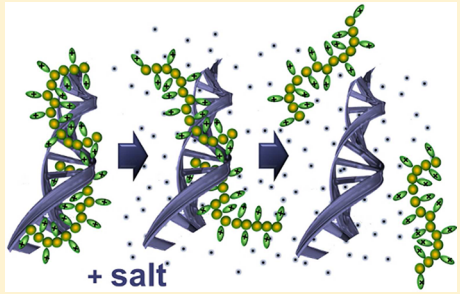


## INTRODUCTION

Complexes of charge bearing polymers, polyelectrolytes (PEs), are versatile materials with applications ranging from industrial solubilization and separation to drug delivery including gene therapy by DNA–polycation complexes. Closely related PE multilayers[1] are used, for example, as responsive coatings, as sensing elements, and in tissue engineering. For reviews, see, e.g., refs 2 and 3. PE complexes are known to be sensitive to added salt with responses including shrinking, under some conditions flocculation or swelling, and at higher concentrations loosening, and finally complete dissociation of the complex.[4,5] Furthermore, salt has been linked to the solubility,[6] kinetics,[7] and composition[8,9] of PE complexes and, specifically, a correlation between the cell transfection of DNA delivered as DNA–PE complexes and the tolerance of the complex to the addition of salt has been suggested.[10]

Excess salt can be used to drive PE multilayers into an exponential growth region,[11] indicating a change in PE chain dynamics, and salt has been reported to be able to dissolve PE multilayers.[12,13] The proposed mechanism is salt ion activated dissociation of contacts between opposite charges in PEs,[12,14] but no direct evidence of the mechanism has existed. Here, we show the salt-driven dissociation of a PE complex by comprehensive atomistic molecular dynamics simulations. We demonstrate the involved mechanism, and isolate the contributing factors. To the best of our knowledge, this is the first study to describe a dynamical transition and capturing the mechanism in full atomistic detail in a PE system. The studied system is a DNA–polylysine (PLL) complex which is one of the most studied polyplectic carriers for DNA delivery with interest in efficiency of target reaching, release dynamics, and mechanics.[15,16]

Most experimental work on DNA–PLL salt response is close to physiological salt concentrations and with excess NaCl. High NaCl concentration has been reported to bring forth swelling and loosening of PLL–DNA complexes with 0.8 M NaCl inducing a melting transition.[4] Formation of isotropic DNA–PLL solution at high NaCl concentrations is also mentioned.[4] Reference 17 maps the DNA–polycation response to NaCl at a soluble–insoluble complex region. Specifically related to PLL–DNA complex salt responses, ref 18 reports a NaCl concentration of 0.86 M to dissociate half of the DNA–PLL complexes, whereas no complexes are present at 1.3 M NaCl. For divalent $MgCl_2$, the corresponding concentrations are 0.2 and 0.5 M.

On the theoretical side, electrostatic interactions joined with counterion release entropy and water binding influence are in general thought to be contributing factors to complex stability. Voorn and Overbeek did the pioneering work in describing PE complexes by combining electrostatic free energy of the complex with Flory–Huggins mixing entropy.[19] Castelnovo and Joanny employ a statistical mechanics approach to describe the complexation.[20] Biesheuvel and Cohen Stuart have taken the Voorn and Overbeek work further by differentiating between the ionic and polymeric charges and their characteristics achieving theoretical stability diagrams in qualitative

Received: December 19, 2013
Revised: February 7, 2014
Published: February 21, 2014





dx.doi.org/10.1021/jp4124293 | J. Phys. Chem. B 2014, 118, 3226–3234

agreement with experiments in relation to mixing ratio and salt concentration.[21] The interplay of counterions and elasticity of the PE has been linked to the complex stability by Schiessel et al.[22]

Furthermore, Ou and Muthukumar[23] conclude on the basis of Langevin dynamics simulations and theoretical considerations that, at weak Coulomb interaction strength, salt affects the PE complexation through screening the Coulomb attraction between PEs. However, in strongly interacting systems, the salt effect on complexation originates from the suppression of the counterion release entropy with the Coulombic energy change in complexation acting against the complexation.

Hence, the ion distribution around PEs is an important factor determining complex formation and its stability. The most known theoretical approach to ion condensation around PEs is by Manning and Oosawa and based on the mean-field Poisson−Boltzmann equation.[24,25] Notably, Sharp has elaborated the Manning picture by investigating the effect of salt in the polyelectrolyte electrostatics through the nonlinear Poisson−Boltzmann equation.[26] More recently, the Manning mean field picture has been shown to break down in the presence of additional divalent salt, or strongly interacting systems.[27−30] In particular, a number of numerical and theoretical approaches in which the PE is defined as a rigid rod or a line charge with varying charge density,[27,31] or a flexible chain of beads,[32] highlight the role of charge correlations in determing the ion condensation around PEs in general, and specifically around the relatively highly charged double stranded DNA. Furthermore, charge reversal upon ion condensation at high enough ionic strength or valency is reported in refs 27, 28, and 32. The importance of charge correlations in divalent ion condensation has also been indicated experimentally.[33]

Besides ion condensation (in terms of total condensed ions), charge correlations are important also in ion binding (in terms of binding sites and dynamics). Therefore, PE complexation and complex stability are likely to be affected by charge correlations at the microstructural level. This is also indicated by refs 34−36, where correlations among bound ions are shown to have a drastic effect on the interactions between two like charged polyions. However, this level detailed studies are still very limited in number and extent: Prior characterization of DNA−PLL complexes encompasses the complex formation and its basic structural characterization.[37,38] Notably, Ouyang et al. make an attempt at characterizing the binding strength of PLL to RNA.[39] Our study here presents, to our knowledge, the first microstructurally detailed study of PE complex dissociation taking PE characterization studies of atomistic detail level to cover also dynamics and transitions for the first time.

## METHODS

**Simulation Model.** All simulations were performed using the GROMACS 4.5.5 simulation package[40] with the empirical Amber99bsc0[41] force field. The Amber bsc0 revision is an improved description of $\alpha/\gamma$ dihedrals in nucleic acids, which ensures the stability and realistic conformations of the DNA oligomer during the full 200 ns of simulation. Earlier AMBER parametrizations have been shown to have problems in these respects.[41−43] For $Na^+$ and $Cl^-$ ions, the Joung and Cheatham ion model[44] was used. The Joung−Cheatham model for the monovalent ions was employed to prevent the unrealistic crystallization observed with standard Amber99 ions in high salt concentrations.[45,46] As $Ca^{2+}$ is not available in the Joung and Cheatham ion model, the standard Amber $Ca^{2+}$ ion model was utilized.[47] This choice was made to ensure $Ca^{2+}$ parametrization compatibility with the DNA and PLL parametrizations. We note different ion parametrizations differ in ion condensation and values reported in this work should be regarded qualitatively, although the ions in this work do not crystallize in the simulations and decomplexation concentrations are in line with experimental salt concentrations for decomplexation. In compliance with the Amber force field, TIP4P-Ew water model[48] was used.

Periodic boundary conditions in all three directions and full particle mesh Ewald (PME)[49] in calculating the long-range electrostatic interactions were utilized in the simulations. For the PME algorithm, a real space cutoff of 1.2 nm and Fourier spacing of 0.12 nm were used, while the simulation package was allowed to determine the optimal grid spacing in the reciprocal space. Lennard-Jones potentials were cut off at 1.0 nm with a shifting function between 0.8 and 1.0 nm. No long-range dispersion correction was applied. LINCS[50] constraints for bonds involving hydrogen were used in the simulations, while the equations of motion were integrated with a time step of 2 fs. The Parrinello−Rahman[51] barostat and Nosé−Hoover[52,53] thermostat were used with a reference temperature of 300 K and a pressure of 1 bar. The time constants were $\tau_T$ = 0.1 ps and $\tau_p$ = 2 ps for the thermostat and barostat. All presented simulation snapshots were generated using VMD.[54]

**Simulated System.** The DNA molecule used in the simulations is the Drew−Dickerson dodecamer d-(CGCGAATTCGCG). This double stranded DNA oligomer carries a net charge of −22e. The PLL in the simulations is a linear polypeptide consisting of 20 fully protonated lysines. The N-terminal residue charge is +2e, and the C-terminal is neutral totalling to a PLL net charge of +20e. The backbone of the PLL is the most hydrophophic part of the PE. To study the complexation and decomplexation of the DNA oligomer with the polycation, the DNA and two PLL molecules were placed into a simulation box of 10 × 10 × 10 $nm^3$ and solvated with water molecules. A sufficient number of counterions to neutralize the system was added by replacing water molecules. As a consequence, the salt-free systems contain 22 $Na^+$ (or 11 $Ca^{2+}$ ions) for DNA and 40 $Cl^-$ ions for the two PLLs. When excess salt is present, the countercations are the same species as the excess salt cation.

To ensure the complexed structure and the complexation process are independent of the initial configuration, several starting configurations with well-separated DNA and PLL at various orientations and separations of the molecules were used. The complex formation and structures obtained were insensitive to the choice of initial configuration. To map out the effect of salt concentration and valency on the complex, a representative complexed configuration formed in the absence of excess salt was introduced to NaCl and $CaCl_2$ concentrations of 0.13, 0.27, and 0.52 M for both salt types. Additionally, 0.39 M $CaCl_2$ and 1.04 M NaCl were studied to complement the data set. Simulations with and without salt were run for 200 ns. In addition, the DNA was studied in the absence of the oppositely charged polyelectrolyte at the same excess salt concentrations for 80 ns.

## RESULTS AND DISCUSSION

In the absence of added salt, the two PLLs both rapidly complex to the DNA segment. The contact between the PLL and DNA is zipper-like with the positive nitrogen $NH_3^+$ ends of


dx.doi.org/10.1021/jp4124293 | J. Phys. Chem. B 2014, 118, 3226−3234

PLL mainly attached to the negative phosphate oxygens (OP) of the DNA; see Figure 1. The PLL binding is dominated by

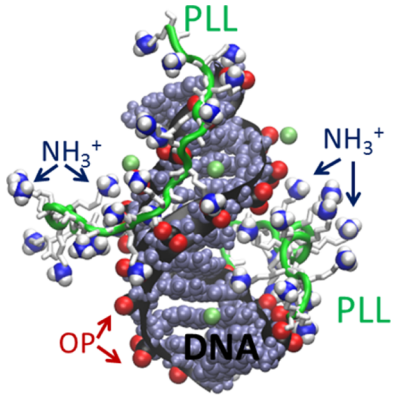


**Figure 1.** The DNA–PLL complex. The site labels show the DNA backbone phosphate oxygen (OP) and PLL side chain $NH_3^+$ sites. The visualization omits for clarity the ions and the water molecules present in the simulation.

the charged nature of the PLL; i.e., no co-operativity due to hydrophobicity is observed. Once formed, the complex is extremely stable and PLL distribution rather even on the DNA surface. However, the PLL chains do sample a number of binding configurations. The most frequent binding configuration has one of the PLLs residing in the major groove and the other either loosely on top of the minor groove or attached to both the minor and major groove with the PLL backbone parallel to the axis of the DNA. The binding behavior and binding stability are insensitive to the starting configuration. Our observations on the structure and formation of the complex in the absence of excess salt are in agreement with ref 37, where DNA complexation with a single PLL molecule was studied in comparable detail with 12–18 ns simulations.

The addition of salt changes the situation. Figure 2 shows the average of PLL backbone nitrogen atom distances to the closest

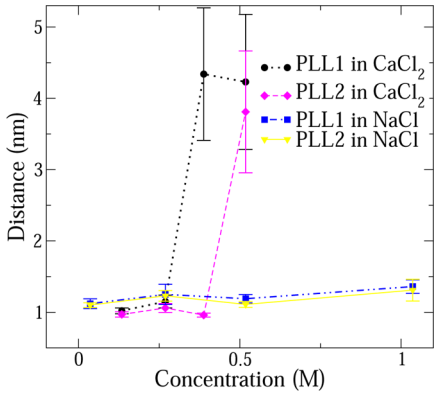


**Figure 2.** The average of PLL backbone nitrogen atom distances to the closest DNA atom at varying concentrations of NaCl and $CaCl_2$ during the last 100 ns of the simulations. Fluctuations in the distance are presented as error bars (one standard deviation from the mean).

DNA atom at varying concentrations of NaCl and $CaCl_2$. As expected, added monovalent salt acts to destabilize the complex but the complex is relatively insensitive to added monovalent salt at concentrations below 1.04 M. With divalent salt, the behavior is drastically different: 0.36 M $CaCl_2$ leads to full detachment of one of the PLLs from the DNA and 0.52 M $CaCl_2$ to a complete dissociation of the complex. This could represent the thermodynamic partitioning transitioning from complete complexation via partial complexation to dissociation or, as very likely in the case of 200 ns simulations, represent metastable simulation configurations. The PLL attached to the major groove is typically the PLL fluctuating more and detaching first. In the major groove binding site, the PLL needs to stretch its side chains more to close the zipper to the DNA OP sites. This stretching is energetically costly, as it results in the loss of flexibility and configurational entropy. Weaker binding to the major groove has been reported earlier for PLL and RNA in the absence of added salt.[39]

The detachment occurs gradually with a self-healing zipper-like mechanism; see Figure 3. The cations condensing to the

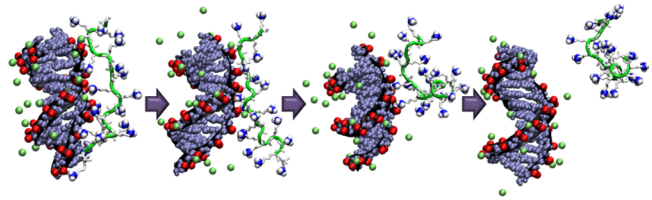

**Figure 3.** Detachment of the PLL chain from the DNA driven by 0.52 M $CaCl_2$ concentration. $Ca^{2+}$ ions within 1 nm of the DNA are shown in green, phosphate oxygens in red, and nitrogen tips of the PLL residues in blue. To show the detachment mechanism more clearly, the visualization omits the second PLL chain which also detaches in the simulation, all Cl ions, and water molecules.

negative OPs of the DNA compete with the $NH_3^+$ tips of the PLL side chains. The flexibility of the PEs and the mobility of the ions determine the dynamics, but at sufficient ion condensation, the zipper formed by DNA and PLL slowly opens. This is quantified by Figure 4 which shows the increase of the number of $Ca^{2+}$ ions condensed to DNA OP sites, while the number of contacts between the PLL $NH_3^+$ and DNA OP sites decreases in the 0.52 M $CaCl_2$ system. The opening of the PLL–DNA zipper is likely a reversible process, but in the simulations, the complexation in the absence of salt occurs so

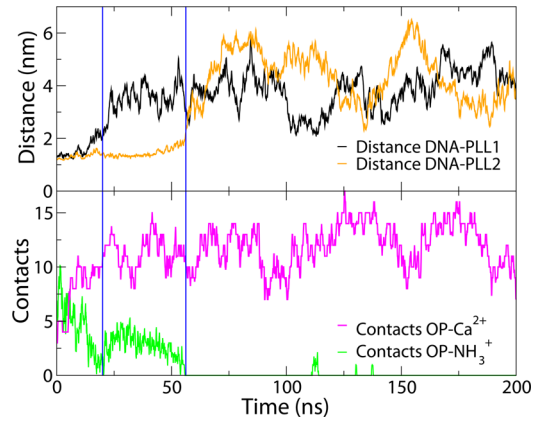


**Figure 4.** (top) The average PLL backbone nitrogen atom distances to the closest DNA atom. (bottom) The number of contacts between the DNA phosphate oxygens (OP) and the $Ca^{2+}$ ions, and between OP sites and PLL nitrogen ends ($NH_3^+$) at 0.52 M $CaCl_2$. A cutoff of 0.35 nm has been used for defining contacts. The vertical lines show the time of detachment for the two PLLs (time of last DNA–PLL contact).


dx.doi.org/10.1021/jp4124293 | J. Phys. Chem. B 2014, 118, 3226–3234

rapidly that we are unable to directly observe the complexation mechanism.

Why is $CaCl_2$ much more efficient in driving dissociation? First, regardless of salt concentration, the number of $Ca^{2+}$ ions condensed to DNA in the simulations is 130−190% of the number of condensed $Na^+$ ions; see Figure 5. The difference in

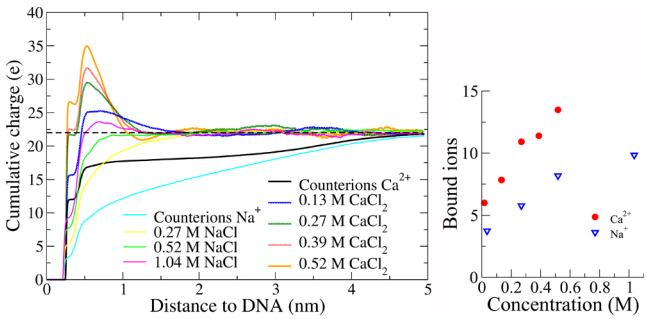


**Figure 5.** (left) The cumulative charge distribution around DNA without and with excess salt as a function of distance to the closest DNA atom calculated from the simulation trajectories. The dashed line shows the level at which overcharging takes place as the DNA charge is −22e. (right) The corresponding number count of ions within 0.32 nm of DNA. The last 30 ns of the simulation are used in the analysis.

condensed charge is even larger due to valency. Second, the $Ca^{2+}$ binds to the same DNA phosphate oxygen sites that also the PLL $NH_3^+$ side chains prefer upon complexation: $NH_3^+$−OP contacts account for 71% of all the contacts between DNA and PLL and an impressive 95% of all $Ca^{2+}$ in direct contact with DNA bind to the same DNA phosphate oxygens. However, $Na^+$ is not as selective in its binding, as it binds also to the DNA base nitrogens and oxygens deeper in the DNA grooves. Only 65% of the condensed $Na^+$ ions associate with the phosphate oxygens. We note ion size is a contributing factor to the binding site selectivity.[55] As hydrated $Ca^{2+}$ is larger than $Na^+$, it cannot reach the basic O/N sites, buried in the grooves of the DNA. Instead, it binds to the exposed OP sites that also the $NH_3^+$ side chains prefer.

The microscopic binding site discussion is generalized to ion condensation landscape by charge distribution around DNA in Figure 5. $Na^+$ and $Ca^{2+}$ result in very different charge distributions, both qualitatively and quantitatively with the charge distribution forms characterized by two inflection points. The first one around 0.3−0.4 nm corresponds to the cation binding to DNA (finite size of the ions) and defines the primary condensation peak, and the second, faint one, around 0.5−0.6 nm in monovalent salt and $Ca^{2+}$ counterions can be associated with the Manning condensation radius.[27,56] All studied excess $Ca^{2+}$ concentrations result in charge reversal due to secondary condensation. Furthermore, 0.27 M $CaCl_2$ is sufficient to completely neutralize the DNA with primary condensation. At 0.39 M and higher concentrations, charge reversal due to primary condensation takes place. For NaCl, primary overcharging is not observed and only the highest concentration of 1.04 M excess NaCl system exhibits weak secondary overcharging showing resemblance to $CaCl_2$ charge distribution. In particular, the primary condensation is much weaker for $Na^+$ than for $Ca^{2+}$, which has a pronounced tendency to condense near the DNA surface.

Can the higher propensity of $Ca^{2+}$ to condense to DNA be explained by simple arguments? To answer this, we compare the results from our all atom simulations to models relying on simplified continuum electrostatics, with the DNA described as a charged rod. Even in the most simplistic Manning condensation framework[24] with no added salt, a higher condensation of divalent ions to the DNA is predicted. Our results match this qualitatively, but the ion condensation to DNA in our simulations is below Manning: at a distance of 0.7 nm, which corresponds to the Manning radius in a salt free system, 48% of the DNA charge for monovalent and 78% for divalent counterion is neutralized. The Manning predictions are 76 and 88%, respectively. This can be explained by the limited length of our DNA, as end effects could be significant. Also, the double-groove structure of the atomistic DNA has been suggested to decrease the condensation.[26] Sub-Manning condensation around DNA has been reported in previous molecular dynamics simulations with explicit water.[55] Undoubtedly, also the choice of the ion description in the force field causes some variance in the precise amount of condensed ions.[57]

In low monovalent salt, our charge distribution shapes match qualitatively the distribution shapes obtained in ref 27 describing the PE as a charged cylinder in implicit solvent environment with excess ions. A similar kind of qualitative match between Poisson−Boltzmann theory and explicit water all-atom molecular dynamics for monovalent salt has been reported before[56] with the use of a simple potential to describe the hydration effect. In particular, refs 27 and 56 discuss the inflection points and their relation to ion condensation.

However, increasing concentration and valency gives rise to correlation effects, which cannot be explained by mean field descriptions. Even though the relationship between correlations and overcharging has been investigated extensively[58,59] with theoretical models and more coarse-grained simulations, work explicitly showing these correlations with atomistically detailed models, like here, remains scarce. In our simulations, the appearance of overcharging already with our lowest concentration of added divalent salt (0.13 M $CaCl_2$) and high concentration of monovalent salt (1.04 M NaCl) is a direct evidence of the presence of these correlations. The layering of the ions at 0.27−0.52 M $CaCl_2$, visible as the decrease in the magnitude of the cumulative charge after the primary condensation peaks and the shifting of the secondary positive condensation layer closer to the DNA with increasing salt condensation, is a second direct indication of correlations in our simulation system. The double-layering of ions is caused by the $Cl^-$ co-ion condensation, and a similar effect has been reported in studies where the PE is described as a charged cylinder[27] and by Wigner crystal based theory.[60] Furthermore, the shift of secondary overcharging peaks with increasing salt has been observed in ref 28. Hence, as the salt concentration and valency increase, the correlations start to dominate the characteristics of the charge distribution around the DNA and the predictive power of mean-field Poisson−Boltzmann electrostatics decreases. To capture the correlation effects, more complex descriptions are required, as also noted by refs 28, 33, 60, and 61. In particular, similar valency induced correlation effects as observed in our work have been suggested to be behind the pronounced ability of divalent ions to condense to DNA.[33,61]

An analogous analysis of the DNA−PLL complex charge distribution reveals that, during the complexation, the PLL rapidly drives away the counterion cloud of the DNA. Hence, the PLL dominates the charging near the DNA surface; see Figure 6. The counterions are further away from the DNA


dx.doi.org/10.1021/jp4124293 | J. Phys. Chem. B 2014, 118, 3226−3234

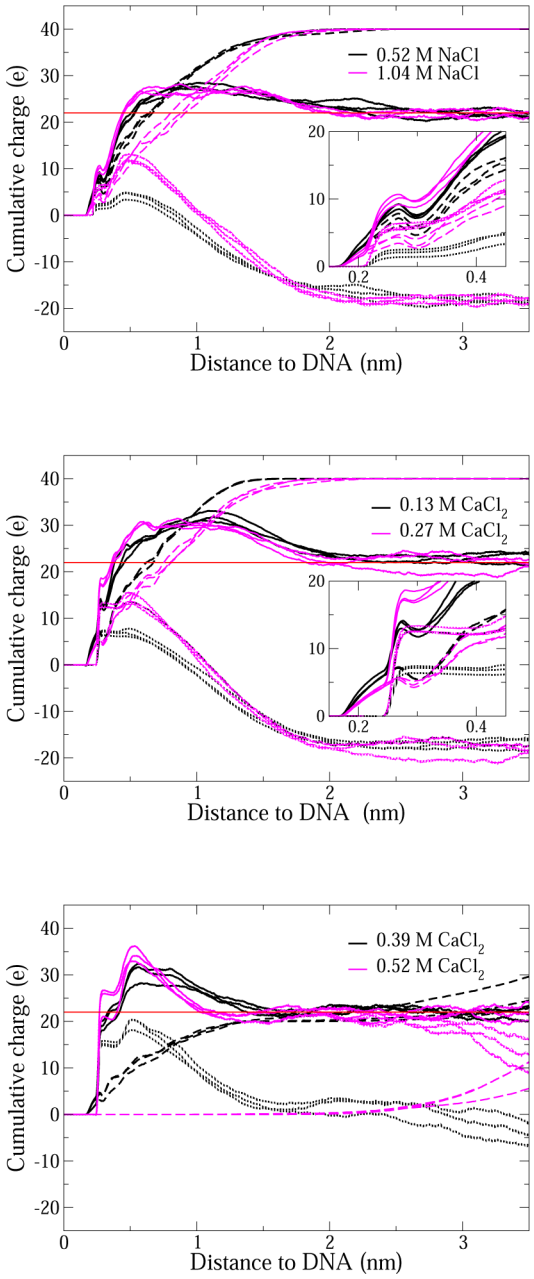


**Figure 6.** Cumulative charge distribution around DNA for the DNA–PLL complex at 0.52 and 1.04 M NaCl (top figure, both PLLs complexed), 0.13 and 0.27 M $CaCl_2$ (middle figure, both PLLs complexed), and 0.39 and 0.52 M $CaCl_2$ (bottom figure, one or both PLLs detached). Charge distribution is calculated from the simulation trajectories as an average over 5 ns in time with the three data lines for each plotted charge distribution demonstrating the time variation in the data. Total charge is plotted as a solid line, counterion contributions by a dotted line, and PLL charge by a dashed line. Distance is measured as the distance to the closest DNA atom.

surface and gradually neutralize the DNA–PLL complex. Increasing the NaCl concentration induces both a rising ionic contribution inside the complex and a shift of the PLL charge contribution to further away from the DNA surface. With $CaCl_2$, the same effect is achieved with much lower concentrations and we stress that also the ionic strengths of the solution are lower for $CaCl_2$. At 0.13 M $CaCl_2$, significantly more ion charge has pushed into the complex compared to 0.52 M NaCl. Comparing 0.27 M $CaCl_2$ and 1.04 M NaCl, one sees that, while the amount of ionic charge in the complex is only slightly more in 0.27 M $CaCl_2$, $CaCl_2$ presents a strikingly pronounced primary condensation compared to NaCl. We note these differences in the amount of condensed $Na^+$ and $Ca^{2+}$ ions and the resulting charge distribution shapes within the complex well preserve the charge distribution behavior observed in the case of DNA without the PLL.

The ion charge pushing the PLL charge distribution cloud further from the DNA in Figure 6 is a sign of binding loosening and fluctuations in the simulations. Already a 0.13 M $CaCl_2$ concentration causes the PLL to partially detach for short periods in the molecular dynamics simulation (reversible unzipping), moving the average PLL charge cloud further from the DNA. Increasing the $CaCl_2$ concentration to 0.27 M and above further enhances this loosening systematically. For NaCl, a 1.04 M concentration is required to significantly loosen the complex. See the Supporting Information for the complete set of DNA–PLL distance data as a function of time.

The total charge distribution of the DNA–PLL complex, Figure 6, presents a charge reversal. This charge reversal peak increases only moderately in height with increasing salt concentration. When decomplexation finally takes place, and $Ca^{2+}$ replaces PLL as the cationic component neutralizing the DNA charge, the charge reversal peak becomes much more localized and moves closer to the DNA. This means that DNA charge is neutralized more effectively and at a shorter distance. Furthermore, upon full decomplexation, the analoguos DNA-only system charge distribution is recovered in the vicinity of DNA.

On the basis of the similarities of the ion charge distributions between DNA-only and the complexed system, we propose that the secondary overcharging region between 0.4 and 0.6 nm in DNA-only systems (Figure 5) could correspond to the PLL charge cloud moving to a larger distance from the DNA in Figure 6. This is accompanied by increased fluctuations in the DNA–PLL complex structure and causes the complex to loosen. Finally, stable PLL decomplexation is observed in the simulations at the precise concentration where added divalent salt concentration first results in primary overcharging in the DNA-only simulation. This overcharging takes place between 0.3 and 0.4 nm distance from the DNA (measured to the closest DNA atom) and is thus much closer to the DNA than the secondary overcharging region. We note that the simulation duration of 200 ns is a short period if there is a significant kinetic barrier opposing detachment—we cannot conclude whether secondary overcharging observed at lower divalent charge concentrations and at the 1.04 M NaCl concentration associated with the loosening of the complex in the simulations would be sufficient to cause detachment, or partial detachment, given more time. However, correlation induced primary overcharging leads to definite PE complex dissociation in the simulations. Microscopically, the occurrence of primary overcharging corresponds to over 1/4 of the OP sites being blocked by $Ca^{2+}$ in direct contact.

To conclude the electrostatics discussion, our results fully support the claims[33,61] that electrostatics and ion correlations play a significant role in divalent ion condensation to DNA. We also showed that characteristic charge distribution shapes were well preserved between DNA-only simulations and the DNA–PLL complexes near the DNA surface. Therefore, we suggest that electrostatics and in particular the correlation effects are in a key role also in the PE complex dissociation we observe.


dx.doi.org/10.1021/jp4124293 | J. Phys. Chem. B 2014, 118, 3226–3234

To back up this claim, we point out that the ability of $CaCl_2$ to dissolve the DNA−PLL complex cannot solely be explained by a simplistic argument of more effective screening between the opposite sign polyelectrolytes. Even though the Debye length of the system is indeed strongly dependent on the valency of the salt, the Debye length both in 1.04 M NaCl and 0.52 M $CaCl_2$ is in the order of the ion radius and differs between the systems only by 0.5 Å. Despite this, the $CaCl_2$ rapidly dissociates the complex, whereas the NaCl only induces fluctuations and loosening. A similar conclusion on the role of screening has been made in the case of strongly charged PEs by Ou and Muthukumar.[23]

So far, we have concentrated on the charge correlations and the role of electrostatics in our discussion. Ion condensation is indeed considered to be governed by electrostatics by many,[56,62,63] but others emphasize factors like the role of water.[64−67] Particularly interesting is the work by Sinn et al.[64] where they conclude that the condensation of $Ca^{2+}$ to polyacrylate is purely driven by the release of waters from the hydration shell of the ion upon binding. In comparison to bulk water, the water molecules in hydration shells of the PEs or the ions have reduced degrees of freedom. Because of this, releasing water produces a favorable entropy contribution to free energy.

To see whether water could provide an additional driving force for $Ca^{2+}$ condensation, we investigated the changes in $Na^+$ and $Ca^{2+}$ hydration shells upon binding to the OP sites. As expected, $Ca^{2+}$ ion binds more water molecules than $Na^+$; see Table 1. Upon binding, both lose water molecules especially

**Table 1. The Average Number of Water Molecules in the Hydration Shells of $Na^+$ and $Ca^{2+}$ Ions in Bulk Solution and Bound to the DNA Phosphate Oxygen and the Difference in Water Molecules Released upon Ion Binding**

| | $H_2O$ bulk ions | $H_2O$ bound ions | $\Delta H_2O$ |
|---|---|---|---|
| $Na^+$ (first shell) | 5.78 | 4.59 | 1.19 |
| $Ca^{2+}$ (first shell) | 8.87 | 7.76 | 1.11 |
| | | **$\Delta H_2O$ released** | **0.08** |
| $Na^+$ (second shell) | 17.94 | 15.03 | 2.91 |
| $Ca^{2+}$ (second shell) | 21.75 | 18.27 | 3.48 |
| | | **$\Delta H_2O$ released** | **−0.57** |

from their second hydration shell. In absolute numbers, we observe a release decrease of 4.6 waters from the vicinity of $Ca^{2+}$ upon binding, whereas Sinn et al. approximate the number of released waters in the case of polyacrylate to be 10.

That said, the difference in average water release between the ions is small: $Ca^{2+}$ loses 0.6 water molecules more than $Na^+$ from its second hydration shell. However, the water molecules around $Ca^{2+}$ are more oriented and they also retain the orientation better upon binding to OP, indicating more restricted degrees of freedom; see Figure 7. We interpret this as a sign of more entropy being gained per released water molecule in the case of $Ca^{2+}$ compared to $Na^+$: the hydration component of the free energy is indeed more favorable to $Ca^{2+}$ binding.

Finally, the systems with monovalent and divalent ions have an interesting kinetic difference influencing the expected rates: the average lifetime of the $Ca^{2+}$−OP bond is at least an order of magnitude longer than the $Na^+$−OP bond lifetime calculated from our simulations. Consequently, a $Ca^{2+}$ ion condensed to DNA lingers at the binding site and blocks a PLL $NH_3^+$ group from attaching. $Na^+$ is more dynamic with its contacts, and

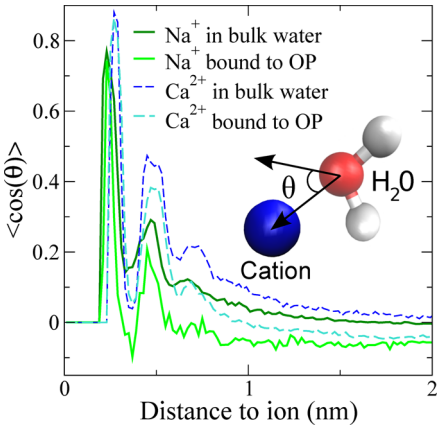


**Figure 7.** Average orientation of water molecules in $\langle \cos\theta \rangle$ as a function of the distance from the cation center of mass. $\theta$ is the angle defined by water dipole and the ion position with respect to water oxygen; see inset. The orientation is shown for both ions in bulk water and ions bound to the DNA OP sites.

therefore less effective in blocking the PLL, as faster detachment of the ion enables more frequent recovery of DNA−PLL zipper contacts. In contrast, the loosening of the DNA−PLL structure due to the lifetime of $Ca^{2+}$−DNA contact allows even more $Ca^{2+}$ ions to condense, resulting in larger fluctuations and, with some concentrations, complete detachment. Kinetic considerations are, however, insufficient to explain the pronounced decomplexation ability of the $Ca^{2+}$ as the kinetics influence the transition frequency between different states but not their actual population in equilibrium.

Related to this, salt is known to accelerate dynamics processes in PE complexes, resulting in, e.g., faster equilibration[14,68] or exponentially growing PE multilayers.[11] An activated dissociation of charge connections has been proposed to govern the relaxation dynamics of PE complexes based on rheology data measurements with salt and temperature promoting in a similar way charge connection dissociation.[14] Here we have show this happens at the microscopic scale: $Ca^{2+}$ lingers at binding sites, breaking the charge connections holding PLL and DNA together. On the other hand, exponential growth of PE multilayers is considered to be related to enhanced diffusion of polyelectrolytes during adsorption.[69−73] The ionic strength activated charge connection breaking between the PEs presented here undoubtedly increases the interchain diffusivity. In addition, the existence of a glass transition ionic strength, where a critical solution ionic strength changes a PE multilayer from glassy to rubbery, has been reported.[74] The PE−PE contact pair breaking we observe could bear a direct connection to such a structural transition at ionic strengths below dissociation.

In summary, both electrostatics correlations and hydration play toward the divalent $Ca^{2+}$ being more effective in condensing to DNA and inducing the decomplexation. Our results of $Ca^{2+}$ driving the dissociation much more effectively than monovalent $Na^+$, and our concentrations of loosening and detachment, are in line with the experimental dissociation results of ref 18, where the divalent ion studied is $Mg^{2+}$. However, $Mg^{2+}$ has been reported[75] to bind to the same OP site that $Ca^{2+}$ binds to in this work, and the ions are close to each other in the Hofmeister series, indicating similar hydration behavior. We note the dissociation concentrations reported match excellently with ours even with the DNA and PLL


dx.doi.org/10.1021/jp4124293 | J. Phys. Chem. B 2014, 118, 3226−3234

molecules in the experiments being significantly larger than in our simulations.

## CONCLUSION

We report the mechanism of salt induced unzipping of a PLL−DNA complex in which the PLL−DNA contacts are replaced by ion condensation to the DNA surface. To our knowledge, this is the first direct evidence of PE−PE charge contact pair breaking induced PE complex loosening. Besides matching experimental loosening and dissociation of the PLL−DNA complex, the results connect directly with the activated dissociation of charge−charge connections proposed to be at the root of a number of PE multilayer properties and could bear wide significance in understanding PE multilayer structure and dynamics.

## ASSOCIATED CONTENT

### Supporting Information

Animations of DNA−PLL complexation and the complex dissociation. Time development of the minimum contact distances corresponding to the average distances presented in Figure 2 showing more in detail the fluctuations and precise detachment. This material is available free of charge via the Internet at http://pubs.acs.org.

## AUTHOR INFORMATION

### Corresponding Author

*E-mail: maria.sammalkorpi@aalto.fi.

### Notes

The authors declare no competing financial interest.

## ACKNOWLEDGMENTS

The authors thank Prof. Kari Laasonen, Prof. Paul Van Tassel, and Dr. Kirsi Yliniemi for useful discussions. This research was supported by National Doctorate Programme in Materials Physics (H.S.A.), Academy of Finland, and a Marie Curie Career Integration Grant within the seventh European Community Framework Programme (grant agreement 293861). Computational resources by CSC IT Centre for Science, Finland, are gratefully acknowledged.

## REFERENCES

(1) Sukhishvili, S. A.; Kharlampieva, E.; Izumrudov, V. Where Polyelectrolyte Multilayers and Polyelectrolyte Complexes Meet. *Macromolecules* **2006**, *39*, 8873−8881.

(2) Cohen Stuart, M. A.; et al. Emerging Applications of Stimuli-Responsive Polymer Materials. *Nat. Mater.* **2010**, *9*, 101−113.

(3) Boudou, T.; Crouzier, T.; Ren, K.; Blin, G.; Picart, C. Multiple Functionalities of Polyelectrolyte Multilayer Films: New Biomedical Applications. *Adv. Mater.* **2010**, *22*, 441−467.

(4) DeRouchey, J.; Netz, R. R.; Radler, J. O. Structural Investigations of DNA-Polycation Complexes. *Eur. Phys. J. E* **2005**, *16*, 17−28.

(5) Dautzenberg, H.; Kriz, J. Response of Polyelectrolyte Complexes to Subsequent Addition of Salts with Different Cations. *Langmuir* **2003**, *19*, 5204−5211.

(6) McLoughlin, D.; McManus, J.; Gorelov, A.; Dawson, K. DNA Complexes with Cationic Surfactant in Mixed Solvents: the Influence of Excess Surfactant and Salt. In *Trends in Colloid and Interface Science XIV*; Buckin, V., Ed.; Springer: Berlin, Heidelberg, 2000; Vol. *115*, pp 186−191.

(7) Kabanov, A. V.; Kabanov, V. A. DNA Complexes with Polycations for the Delivery of Genetic Material into Cells. *Bioconjugate Chem.* **1995**, *6*, 7−20.

(8) Zhou, S.; Chu, B. Assembled Materials: Polyelectrolyte−Surfactant Complexes. *Adv. Mater.* **2000**, *12*, 545−556.

(9) Hayakawa, K.; Santerre, J. P.; Kwak, J. C. T. Study of Surfactant−Polyelectrolyte Interactions. Binding of Dodecyl- and Tetradecyltrimethylammonium Bromide by Some Carboxylic Polyelectrolytes. *Macromolecules* **1983**, *16*, 1642−1645.

(10) Zelikin, A. N.; Putnam, D.; Shastri, P.; Langer, R.; Izumrudov, V. A. Aliphatic Ionenes as Gene Delivery Agents: Elucidation of Structure−Function Relationship through Modification of Charge Density and Polymer Length. *Bioconjugate Chem.* **2002**, *13*, 548−553.

(11) Porcel, C.; Lavalle, P.; Ball, V.; Decher, G.; Senger, B.; Voegel, J. C.; Schaaf, P. From Exponential to Linear Growth in Polyelectrolyte Multilayers. *Langmuir* **2006**, *22*, 4376−4383.

(12) Schlenoff, J. B.; Dubas, S. T. Mechanism of Polyelectrolyte Multilayer Growth: Charge Overcompensation and Distribution. *Macromolecules* **2001**, *34*, 592−598.

(13) Ball, V.; Hubsch, E.; Schweiss, R.; Voegel, J. C.; Schaaf, P.; Knoll, W. Interactions between Multivalent Ions and Exponentially Growing Multilayers: Dissolution and Exchange Processes. *Langmuir* **2005**, *21*, 8526−8531.

(14) Spruijt, E.; Sprakel, J.; Lemmers, M.; Cohen Stuart, M. A.; van der Gucht, J. Relaxation Dynamics at Different Time Scales in Electrostatic Complexes: Time-Salt Superposition. *Phys. Rev. Lett.* **2010**, *105*, 208301.

(15) Park, T. G.; Jeong, J. H.; Kim, S. W. Current Status of Polymeric Gene Delivery Systems. *Adv. Drug Delivery Rev.* **2006**, *58*, 467−486.

(16) Tros de Ilarduya, C.; Sun, Y.; Duezguenes, N. Gene delivery by Lipoplexes and Polyplexes. *Eur. J. Pharm. Sci.* **2010**, *40*, 159−170.

(17) Izumrudov, V. A.; Wahlund, P. O.; Gustavsson, P. E.; Larsson, P. O.; Galaev, I. Y. Factors Controlling Phase Separation in Water-Salt Solutions of DNA and Polycations. *Langmuir* **2003**, *19*, 4733−4739.

(18) Evett, J.; Isenberg, I. DNA-Polylysine Interaction as Studied by Polarization of Fluorescence. *Ann. N.Y. Acad. Sci.* **1969**, *158*, 210−222.

(19) Overbeek, J. T. G.; Voorn, M. J. Phase Separation in Polyelectrolyte Solutions. Theory of Complex Coacervation. *J. Cell. Comp. Physiol.* **1957**, *49*, 7−26.

(20) Castelnovo, M.; Joanny, J. F. Complexation between Oppositely Charged Polyelectrolytes: Beyond the Random Phase Approximation. *Eur. Phys. J. E* **2001**, *6*, 377−386.

(21) Biesheuvel, P. M.; Cohen Stuart, M. A. Electrostatic Free Energy of Weakly Charged Macromolecules in Solution and Intermacromolecular Complexes Consisting of Oppositely Charged Polymers. *Langmuir* **2004**, *20*, 2785−2791.

(22) Schiessel, H.; Bruinsma, R. F.; Gelbart, W. M. Electrostatic Complexation of Spheres and Chains under Elastic Stress. *J. Chem. Phys.* **2001**, *115*, 7245−7252.

(23) Ou, Z. Y.; Muthukumar, M. Entropy and Enthalpy of Polyelectrolyte Complexation: Langevin Dynamics Simulations. *J. Chem. Phys.* **2006**, *124*, 154902.

(24) Manning, G. S. Limiting Laws and Counterion Condensation in Polyelectrolyte Solutions: I. Colligative Properties. *J. Chem. Phys.* **1969**, *51*, 924−933.

(25) Oosawa, F. *Polyelectrolytes*; Dekker: New York, 1971.

(26) Sharp, K. A. Polyelectrolyte Electrostatics - Salt Dependence, Entropic, and Enthalpic Contributions to Free-Energy in the Nonlinear Poisson-Boltzmann Model. *Biopolymers* **1995**, *36*, 227−243.

(27) Deserno, M.; Christian, H.; Sylvio, M. Fraction of Condensed Counterions around a Charged Rod: Comparison of Poisson-Boltzmann Theory and Computer Simulations. *Macromolecules* **2000**, *33*, 199−206.

(28) Deserno, M.; Jimenez-Angeles, F.; Holm, C.; Lozada-Cassou, M. Overcharging of DNA in the Presence of Salt: Theory and Simulation. *J. Phys. Chem. B* **2001**, *105*, 10983−10991.

(29) Trizac, E.; Téllez, G. Onsager-Manning-Oosawa Condensation Phenomenon and the Effect of Salt. *Phys. Rev. Lett.* **2006**, *96*, 038302.

(30) Perel, V. I.; Shklovskii, B. I. Screening of a Macroion by Multivalent Ions: a New Boundary Condition for the Poisson−Boltzmann Equation and Charge Inversion. *Physica A* **1999**, *274*, 446−453.

(31) Nguyen, T. T.; Rouzina, I.; Shklovskii, B. I. Reentrant Condensation of DNA Induced by Multivalent Counterions. *J. Chem. Phys.* **2000**, *112*, 2562−2568.
(32) Kundagrami, A.; Muthukumar, M. Theory of Competitive Counterion Adsorption on Flexible Polyelectrolytes: Divalent Salts. *J. Chem. Phys.* **2008**, *128*, 244901.
(33) Bai, Y.; Greenfeld, M.; Travers, K. J.; Chu, V. B.; Lipfert, J.; Doniach, S.; Herschlag, D. Quantitative and Comprehensive Decomposition of the Ion Atmosphere around Nucleic Acids. *J. Am. Chem. Soc.* **2007**, *129*, 14981−14988.
(34) Arenzon, J.; Stilck, J.; Levin, Y. Simple Model for Attraction between Like-Charged Polyions. *Eur. Phys. J. B* **1999**, *12*, 79−82.
(35) Ha, B.-Y.; Liu, A. J. Counterion-Mediated Attraction between Two Like-Charged Rods. *Phys. Rev. Lett.* **1997**, *79*, 1289−1292.
(36) Ha, B.-Y.; Liu, A. J. Effect of Non-Pairwise-Additive Interactions on Bundles of Rodlike Polyelectrolytes. *Phys. Rev. Lett.* **1998**, *81*, 1011−1014.
(37) Ziebarth, J.; Wang, Y. M. Molecular Dynamics Simulations of DNA-Polycation Complex Formation. *Biophys. J.* **2009**, *97*, 1971−1983.
(38) Elder, R. M.; Emrick, T.; Jayaraman, A. Understanding the Effect of Polylysine Architecture on DNA Binding Using Molecular Dynamics Simulations. *Biomacromolecules* **2011**, *12*, 3870−3879.
(39) Ouyang, D.; Zhang, H.; Herten, D.-P.; Parekh, H. S.; Smith, S. C. Structure, Dynamics, and Energetics of siRNA-Cationic Vector Complexation: A Molecular Dynamics Study. *J. Phys. Chem. B* **2010**, *114*, 9220−9230.
(40) Hess, B.; Kutzner, C.; van der Spoel, D.; Lindahl, E. GROMACS 4: Algorithms for Highly Efficient, Load-Balanced, and Scalable Molecular Simulation. *J. Chem. Theory Comput.* **2008**, *4*, 435−447.
(41) Perez, A.; Marchan, I.; Svozil, D.; Sponer, J.; Cheatham, I.; Thomas, E.; Laughton, C. A.; Orozco, M. Refinenement of the AMBER Force Field for Nucleic Acids: Improving the Description of Alpha/Gamma Conformers. *Biophys. J.* **2007**, *92*, 3817−3829.
(42) Varnai, P.; Zakrzewska, K. DNA and Its Counterions: A Molecular Dynamics Study. *Nucleic Acids Res.* **2004**, *32*, 4269−4280.
(43) Beveridge, D. L.; et al. Molecular Dynamics Simulations of the 136 Unique Tetranucleotide Sequences of DNA Oligonucleotides. I. Research Design and Results on d($C_pG$) Steps. *Biophys. J.* **2004**, *87*, 3799−3813.
(44) Joung, I. S.; Cheatham, I.; Thomas, E. Determination of Alkali and Halide Monovalent Ion Parameters for Use in Explicitly Solvated Biomolecular Simulations. *J. Phys. Chem. B* **2008**, *112*, 9020−9041.
(45) Chen, A. A.; Pappu, R. V. Parameters of Monovalent Ions in the AMBER-99 Forcefield: Assessment of Inaccuracies and Proposed Improvements. *J. Phys. Chem. B* **2007**, *111*, 11884−11887.
(46) Auffinger, P.; Cheatham, I.; Thomas, E.; Vaiana, A. C. Spontaneous Formation of KCl Aggregates in Biomolecular Simulations: A Force Field Issue? *J. Chem. Theory Comput.* **2007**, *3*, 1851−1859.
(47) Aqvist, J. Ion Water Interaction Potentials Derived from Free-Energy Perturbation Simulations. *J. Phys. Chem.* **1990**, *94*, 8021−8024.
(48) Horn, H. W.; Swope, W. C.; Pitera, J. W.; Madura, J. D.; Dick, T. J.; Hura, G. L.; Head-Gordon, T. Development of an Improved Four-Site Water Model for Biomolecular Simulations: TIP4P-Ew. *J. Chem. Phys.* **2004**, *120*, 9665−9678.
(49) Essmann, U.; Perera, L.; Berkowitz, M. L.; Darden, T.; Lee, H.; Pedersen, L. G. A Smooth Particle Mesh Ewald Method. *J. Chem. Phys.* **1995**, *103*, 8577−8593.
(50) Hess, B.; Bekker, H.; Berendsen, H. J. C.; Fraaije, J. LINCS: A Linear Constraint Solver for Molecular Simulations. *J. Comput. Chem.* **1997**, *18*, 1463−1472.
(51) Parrinello, M.; Rahman, A. Polymorphic Transitions in Single-Crystals - a New Molecular- Dynamics Method. *J. Appl. Phys.* **1981**, *52*, 7182−7190.
(52) Nose, S. A Unified Formulation of the Constant Temperature Molecular-Dynamics Methods. *J. Chem. Phys.* **1984**, *81*, 511−519.
(53) Hoover, W. G. Canonical Dynamics − Equilibrium Phase-Space Distributions. *Phys. Rev. A* **1985**, *31*, 1695−1697.
(54) Humphrey, W.; Dalke, A.; Schulten, K. VMD − Visual Molecular Dynamics. *J. Mol. Graphics* **1996**, *14*, 33−38.
(55) Savelyev, A.; Papoian, G. A. Electrostatic, Steric, and Hydration Interactions Favor $Na^+$ Condensation around DNA Compared with $K^+$. *J. Am. Chem. Soc.* **2006**, *128*, 14506−14518.
(56) Heyda, J.; Dzubiella, J. Ion-specific Counterion Condensation on Charged Peptides: Poisson- Boltzmann vs. Atomistic Simulations. *Soft Matter* **2012**, *8*, 9338−9344.
(57) Yoo, J.; Aksimentiev, A. Improved Parametrization of $Li^+$, $Na^+$, $K^+$, and $Mg^{2+}$ Ions for All- Atom Molecular Dynamics Simulations of Nucleic Acid Systems. *J. Phys. Chem. Lett.* **2012**, *3*, 45−50.
(58) Grosberg, A. Y.; Nguyen, T. T.; Shklovskii, B. I. Colloquium: The Physics of Charge Inversion in Chemical and Biological Systems. *Rev. Mod. Phys.* **2002**, *74*, 329−345.
(59) Quesada-Perez, M.; Gonzalez-Tovar, E.; Martin-Molina, A.; Lozada-Cassou, M.; Hidalgo- Alvarez, R. Overcharging in Colloids: Beyond the Poisson-Boltzmann Approach. *ChemPhysChem* **2003**, *4*, 234−248.
(60) Shklovskii, B. I. Screening of a Macroion by Multivalent ions: Correlation-Induced Inversion of Charge. *Phys. Rev. E* **1999**, *60*, 5802−5811.
(61) Chu, V. B.; Bai, Y.; Lipfert, J.; Herschlag, D.; Doniach, S. Evaluation of Ion Binding to DNA Duplexes Using a Size-Modified Poisson-Boltzmann Theory. *Biophys. J.* **2007**, *93*, 3202−3209.
(62) Pack, G. R.; Wong, L.; Lamm, G. Divalent Cations and the Electrostatic Potential around DNA: Monte Carlo and Poisson-Boltzmann Calculations. *Biopolymers* **1999**, *49*, 575−590.
(63) Korolev, N.; Lyubartsev, A. P.; Rupprecht, A.; Nordenskiold, L. Competitive Binding of $Mg^{2+}$, $Ca^{2+}$, $Na^+$, and $K^+$ Ions to DNA in Oriented DNA Fibers: Experimental and Monte Carlo Simulation Results. *Biophys. J.* **1999**, *77*, 2736−2749.
(64) Sinn, C. G.; Dimova, R.; Antonietti, M. Isothermal Titration Calorimetry of the Polyelectrolyte/ Water Interaction and Binding of $Ca^{2+}$: Effects Determining the Quality of Polymeric Scale Inhibitors. *Macromolecules* **2004**, *37*, 3444−3450.
(65) Sinn, C. G.; Dimova, R.; Huin, C.; Sel, Z.; Antonietti, M. Binding of Ion Pairs onto Polymer Gels via Dehydration Entropy: A New Mechanism for Ion Exchange. *Macromolecules* **2006**, *39*, 6310−6312.
(66) Cheng, Y. H.; Korolev, N.; Nordenskiold, L. Similarities and Differences in Interaction of $K^+$ and $Na^+$ with Condensed Ordered DNA. A Molecular Dynamics Computer Simulation Study. *Nucleic Acids Res.* **2006**, *34*, 686−696.
(67) Schlenoff, J. B.; Rmaile, A. H.; Bucur, C. B. Hydration Contributions to Association in Polyelectrolyte Multilayers and Complexes: Visualizing Hydrophobicity. *J. Am. Chem. Soc.* **2008**, *130*, 13589−13597.
(68) Jomaa, H. W.; Schlenoff, J. B. Salt-Induced Polyelectrolyte Interdiffusion in Multilayered Films: A Neutron Reflectivity Study. *Macromolecules* **2005**, *38*, 8473−8480.
(69) Ladam, G.; Schaad, P.; Voegel, J. C.; Schaaf, P.; Decher, G.; Cuisinier, F. In Situ Determination of the Structural Properties of Initially Deposited Polyelectrolyte Multilayers. *Langmuir* **2000**, *16*, 1249−1255.
(70) Salomaki, M.; Vinokurov, I. A.; Kankare, J. Effect of temperature on the buildup of polyelectrolyte multilayers. *Langmuir* **2005**, *21*, 11232−11240.
(71) Hubsch, E.; Ball, V.; Senger, B.; Decher, G.; Voegel, J. C.; Schaaf, P. Controlling the Growth Regime of Polyelectrolyte Multilayer Films: Changing from Exponential to Linear Growth by Adjusting the Composition of Polyelectrolyte Mixtures. *Langmuir* **2004**, *20*, 1980−1985.
(72) Lavalle, P.; Voegel, J.-C.; Vautier, D.; Senger, B.; Schaaf, P.; Ball, V. Dynamic Aspects of Films Prepared by a Sequential Deposition of Species: Perspectives for Smart and Responsive Materials. *Adv. Mater.* **2011**, *23*, 1191−1221.
(73) Lavalle, P.; Vivet, V.; Jessel, N.; Decher, G.; Voegel, J. C.; Mesini, P. J.; Schaaf, P. Direct Evidence for Vertical Diffusion and

Exchange Processes of Polyanions and Polycations in Polyelectrolyte Multilayer Films. *Macromolecules* **2004**, *37*, 1159−1162.
(74) Kovacevic, D.; van der Burgh, S.; de Keizer, A.; Cohen Stuart, M. A. Kinetics of Formation and Dissolution of Weak Polyelectrolyte Multilayers: Role of Salt and Free Polyions. *Langmuir* **2002**, *18*, 5607−5612.
(75) Butler, J. C.; Angelini, T.; Tang, J. X.; Wong, G. C. L. Ion Multivalence and Like-Charge Polyelectrolyte Attraction. *Phys. Rev. Lett.* **2003**, *91*, 028301.